

True stress-logarithmic strain curves test of pipeline steels using 3D digital image correlation

L. Z. KONG^{a,*}, J. SHUAI^a, X. Y. ZHOU^b, K. HUANG^b, G. J. YU^c

^aCollege of Mechanical and Transportation Engineering, China University of Petroleum-Beijing, Beijing 102249, China

^bDepartment of Oil and Natural Gas Engineering, Southwest Petroleum University, Chengdu 610500, China

^cMerchant Marine College, Shanghai Maritime University, Shanghai 201306, China

True stress-logarithmic strain curves of two pipeline steels, API-5L X65 and X90, using the 3D-DIC (digital image correlation) technique were tested. Three methods to obtain the true stress were studied. Method I is based on the displacements of the front and lateral faces of the specimen. Method II, which is based on the longitudinal logarithmic strain, was verified by method I. The results of method II revealed to be smoother and more stable. Method III, which is based on the transverse logarithmic strain, was shown to be invalid after the onset of necking. Six points located in longitudinal and transverse directions of the specimen were studied and the results showed that points' location had little effect on true stress-logarithmic strain curves if the points were on the line of fracture. The material properties of API-5L X65 were compared with those of API-5L X90. API-5L X65 has a higher value of ultimate stress and API-5L X90 has a higher value of ultimate logarithm strain. Comparisons for the yield stress and nominal elongation were also made.

(Received September 12, 2015; accepted October 28, 2015)

Keywords: True stress, Logarithmic strain, Pipeline steel, API-5L X90, Digital Image Correlation

1. Introduction

In current uniaxial tension experiments of pipeline steels, generally an extensometer or a strain gauge is used to obtain the stress-strain curve [1]. MTS, Instron and other material test machines are equipped with an extensometer to acquire the strain in the longitudinal direction. As we all know, the principle of an extensometer acquiring the strain is by dividing the stretched length of the extensometer by its original length. On this account, the obtained strain is an average value of the extensometer section and thus was affected by the extensometer length [2]. What's more, it could not be applied after the onset of necking. For the method of strain gauge, it is mainly applied in the elastic range subject to its range limitation. With the development of strain-based design for pipelines [3, 4], it is increasingly urgent to acquire the full-range stress-strain curves.

The exploration on testing the true stress-strain curves of pipeline steels has lasted for a long time. Before the maturity of the DIC technique, many scholars obtained the true stress-logarithmic curve using physical methods. Li et al. [5] tested the true stress-logarithmic strain curves of API-5L X46, X60, X65 and X80 through detecting the axial and radial displacements of circular cross-section specimen with a displacement meter. The true stress and logarithmic strain were calculated through

the diameter variation of the specimen within the circular cross-section. Later, a method of testing the true stress-logarithmic strain curves of specimens with rectangular cross-section was proposed [6], which tracked the dimensional variations of the mostly necking region with a special extensometer.

Owing to the rapid development of computer technology and the improvement of the resolution of the digital camera lens, the DIC (Digital Image Correlation) technique has been widely used in the field of polymers [7, 8], especially in the material property test of thermoplastics [9, 10, 11]. In the test with the DIC technique, the strain could be directly obtained from DIC results, while the stress was acquired only through further processing.

There are three methods included in calculating the true stress. The first one is based on the displacements of front and lateral surfaces of the rectangular cross-section specimen [11, 12]. The second and third methods are based on the longitudinal and transverse strain, respectively. The first and the third methods were used to test the true stress-logarithmic curves of polymers [11] and results showed that the stress of the third method was far from that of the first method. Leitão et al [13] tested the local constitutive properties of aluminum friction stir welds using the second method. The second method is under the assumption of incompressibility and the third

method is under the assumption of isotropy. Lockwood et al. [14, 15] analyzed the viability of the incompressibility assumption by performing numerical simulations of tensile tests using a FE model. But a full correspondence between predicted and measured global material behaviors was not achieved. In addition, William [16] proposed that the volume incompressibility principle was true at the onset of necking. Many tests with DIC technique, based on the incompressibility or the isotropy assumption, have conducted. However, little attention has been given to the validation of the second or the third method, especially for pipeline steels. Besides, few attempts have been conducted on points' location effect on the second method. In this paper, we aim to test the feasibilities of the second and the third methods and assess the incompressibility and isotropy assumptions. Pipeline steels of API-5L X65 and X90 were tested and Poisson's variation and points' location effect were also studied.

2. Methodology

2.1 Materials and test specimens

The materials investigated in this paper are grades API-5L X65 and X90 pipeline steels, which are widely used in the oil and gas industries. The tensile test specimens, as shown in Fig. 1, of API-5L X65 and X90 are in the same dimensions. The specimen dimensions are designed according to ISO 6892-1-2009 [17] and GB/T 228-2002 [18]. The thickness and the width of the specimen are 8 mm and 20mm, respectively. Six plat specimens in the L-T direction (the L direction is the axial or longitudinal direction of the pipeline, and the T direction is the circumferential or transverse direction of the pipeline) are extracted; three of them are extracted from a pipe section of API-5L X65 and other three are extracted from a pipe section of API-5L X90. The y-direction in Fig. 1 is the longitudinal direction of the pipeline and the x-direction is the transverse direction of the pipeline.

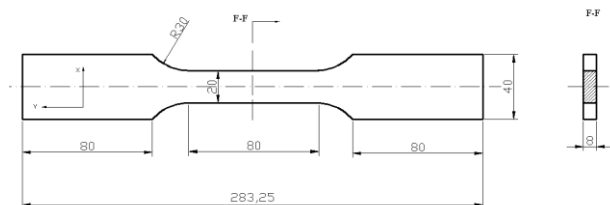


Fig. 1. The sketch of the specimen. y-direction is the longitudinal direction of the pipeline and x-direction is the transverse direction of the pipeline

2.2 Experimental procedure

Uniaxial tension tests were conducted in a MTS 810 universal test machine at 20°C. Specimens were clamped using hydraulic grips mounted on a 250 kN tensile test rig and were loaded in a constant displacement rate mode (2mm/min). The length of the narrow portion of the specimen is 80mm, which results a nominal strain rate of $4 \times 10^{-4} \text{ s}^{-1}$. Specimens were loaded until fracture and the signal was logged using 793.10 multipurpose TestWare. Further post-processing of the crude data was carried out using in-house MATLAB [19] scripts.

2.3 Digital Image correlation

Full field deformation and strain measurements were performed using a digital image correlation system, Vic-3D, which was developed and implemented by Correlated Solutions Incorporated [20]. There are four CCD cameras, as shown in Fig. 2, simultaneously taking pictures of the deforming specimen under the control of an MTS control System, which ensures the synchronization of image capturing and loading. Two CCD cameras, which have a resolution of 2448×2048 pixels, were placed directly in front of the specimen to measure the deformation on the front surface; and the other two cameras, which have a resolution of 1360×1036 pixels, were placed on the right-hand side to measure the deformed profile of the specimen. Four CCD cameras were applied when the stress was calculated by method I (see section 2.5). Only two CCD cameras which were placed directly in front of specimens and were schematically shown in Fig. 3, were applied when the stress was calculated by the method II or III. A random black and white speckle pattern was applied to specimens prior to testing using matte spray paint. The pattern, as shown in Fig. 4, must be painted carefully and optimized to be more fined. One Picture was taken every half second. In addition, a set of pictures was taken of the un-deformed specimens. These pictures were considered as the reference case to determine displacements and strains for all of the subsequent pictures. x, y and z -directions are shown in Fig. 3 such that the x-direction is parallel to the horizontal direction and the y-direction is parallel to the vertical direction. The displacements are determined by correlation of the digital images with an specific software [21]. Basically, the pictures are subdivided in a subset of 19×19 pixels, which is tracked in subsequent images.

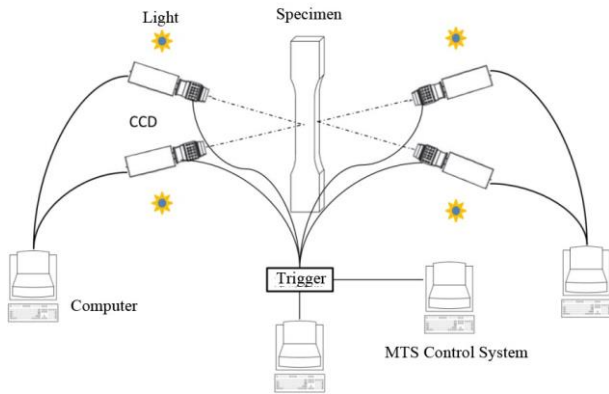


Fig. 2. The Schematic Diagram of DIC Test System with Four CCDs. Two CCDs were placed directly in front of the specimen and the other two CCDs were placed at the right-side of the specimen

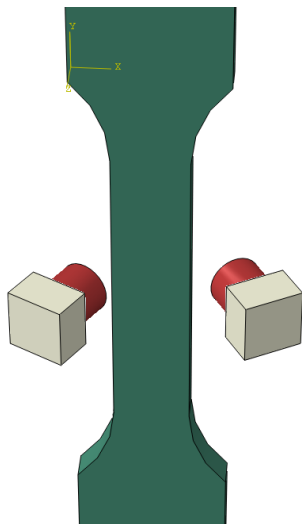


Fig. 3. The Schematic Diagram of DIC Test System with Two CCDs. x-direction is parallel to the horizontal direction and the y-direction is parallel to the vertical direction

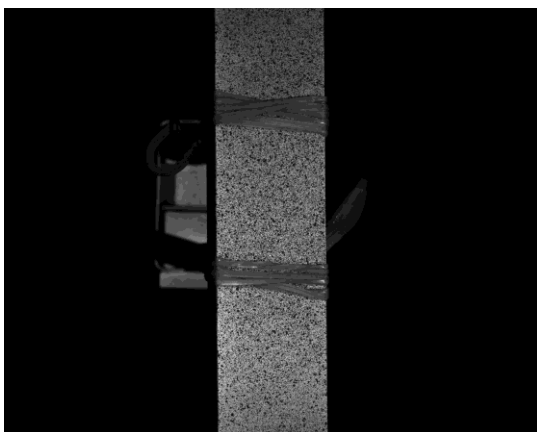


Fig. 4. Example of Speckle Pattern

2.4 Strain calculation

Strains obtained from the 3D-DIC system are average Green-Lagrange strains, which are calculated according to the correlated relation between the pictures of the deformed specimen and reference pictures of the un-deformed specimen. Usually used strains in engineering and research fields are more often the logarithmic strains. So the average Green-Lagrange strains need be converted into logarithmic strains according to Eq. (1) [11]. In which ε_{ii} is the logarithmic strain and \bar{E}_{ii} is the average Green-Lagrange strain in the same direction. The subscript of i could be x, y or z, which are the directions of the specimen shown in Fig. 3 (y is the longitudinal direction, x and z are transverse directions).

$$\varepsilon_{ii} = \frac{1}{2} \ln(1 + 2\bar{E}_{ii}) \quad (1)$$

2.5 Stress calculation

Three methods, which are named as methods I, II and III, for determining the true stress of pipeline steels using the 3D-DIC technique are introduced. Method I, calculating the longitudinal macroscopic Cauchy stress based on the average normal displacements on the front and lateral faces of the specimen [11, 13], is shown as:

$$\sigma_{yy} = \frac{P}{A} = \frac{P}{W \cdot B} = \frac{P}{(W_0 - 2B_x) \cdot (B_0 - 2W_z)} \quad (2)$$

where σ_{yy} is the true stress in the longitudinal direction, P is the current force, A is the current cross-sectional area at the necking section, W and W_0 are the current and initial width of the specimen in the x-direction, B and B_0 are the current and initial thickness of the specimen, B_x is the average displacement in the x-direction of points on the specimen's lateral surface at the necking section and W_z is the average displacement in the z-direction of points on the specimen's front surface at the necking section. Two cameras of 2448×2048 pixels were used to record W_z of the points on the front surface of the specimen while the other two CCD cameras of 1360×1036 pixels were used to record B_x of the points on the lateral surface of the specimen. Then, $W_0 - 2B_x$ and $B_0 - 2W_z$ were used to calculate the current lengths in the x and z -directions. According to the theory of the method I, incompressibility and isotropy assumptions were not needed when calculating the true stress. So method I was reliable.

Method II is based on the longitudinal logarithmic strain. Under the incompressibility assumption, Eq. (3) is established.

$$\sigma = \frac{F}{A} = \frac{F}{A_0} e^{\varepsilon_{yy}} \quad (3)$$

Method III is based on the transverse logarithmic strain. The true stress calculated by the current force (given by the load cell) and the current cross-section area, is given by

$$\sigma = \frac{F}{A} = \frac{F}{A_0} \frac{A_0}{A} = \frac{F}{A_0} \frac{W_0 \cdot B_0}{W \cdot B} = \frac{F}{A_0} e^{-\varepsilon_{xx}} \cdot e^{-\varepsilon_{zz}} \quad (4)$$

where ε_{xx} and ε_{yy} are logarithmic strains in the x-direction and z-direction respectively. On the assumption of isotropy, ε_{xx} equals as ε_{yy} and the calculation formula of the true stress is as:

$$\sigma = \frac{F}{A_0} e^{-2\varepsilon_{xx}} \quad (5)$$

In method III, the current force, the initial cross-section area and the transverse strain are needed for the true stress calculation.

2.6 Bridgman equation

As we all know, the stress state changes from a uniaxial to a triaxial stress state at the onset of necking. So a geometry correction must be applied in order to get a full-range true stress-logarithmic strain curve. It must be noted that the geometry correction is simply applied to the stress, rather than the strain. The same correction procedure with Bridgman equation used for the round tensile specimen can be equivalently used for the correction of the true stress obtained from rectangular tensile specimen, which has been validated by Zhang et al. [6]. For the round tensile specimen, the following correction equation by Bridgman is well known [21]:

$$\sigma_{cor} = \frac{\sigma}{\left(1 + \frac{2R}{a}\right) \ln\left(1 + \frac{a}{2R}\right)} \quad (6)$$

where σ_{cor} is the corrected true stress, σ is the true stress calculated with method I, II or III, a is the current radius of the neck and R is the radius of curvature of the neck surface in the longitudinal plane at the minimum section. The correction starts once the maximum load has passed.

The neck geometry parameter, a/R , was determined by the empirical expression for the neck geometry parameter [22]:

$$\frac{a}{R} = 1.1 \cdot (\varepsilon - \varepsilon_{p_{max}}) \quad (7)$$

where $\varepsilon_{p_{max}}$ is plastic part of the logarithm strain at the maximum load, ε is the logarithmic strain after the onset of necking.

3. Results and discussion

3.1 True stress calculation by methods I and II

Fig. 5 displays true stress-logarithmic strain curves of API-5L X65 steel obtained by method I. Three curves are in a consistent trend. Fluctuations of the true stress exist in the endgame of the stretching process, which are mainly due to the deviation of the recorded displacements before the fracture of the specimen. The transition from elastic stage to elastoplastic stage is smooth in the partially enlarged view in Fig. 5, although it is a little rough in the overall view. The post-peak strain softening phenomenon observed in nominal stress-strain curve did not turn up in the true stress-logarithmic strain curves, which means that the true stress of the pipeline steel is continuously increasing with the strain increment. The strain softening, which is mainly caused by the cross-section area reduction in the necking process, is not representative of the material behavior. The stress correction caused by stress state change in the necking process will be analyzed in Section 3.4.

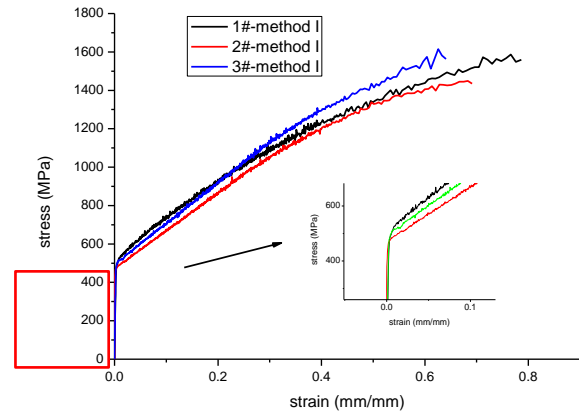


Fig. 5. The true stress-logarithmic strain curves of specimens calculated through method I. The transition from elastic stage to elasto-plastic stage is very smooth in the partially enlarged view

Fig. 6 represents the true stress-logarithmic strain curves of API-5L X65 calculated by method II. The true stress-logarithmic strain curves calculated by methods I and II are in high agreement in the entire strain scope. The bifurcation emerges when the strain is greater than 15.8% for specimen 2# and 18.4% for specimen 3#. The deviation between the results of methods I and II is not very large for specimens 2# and 3#.

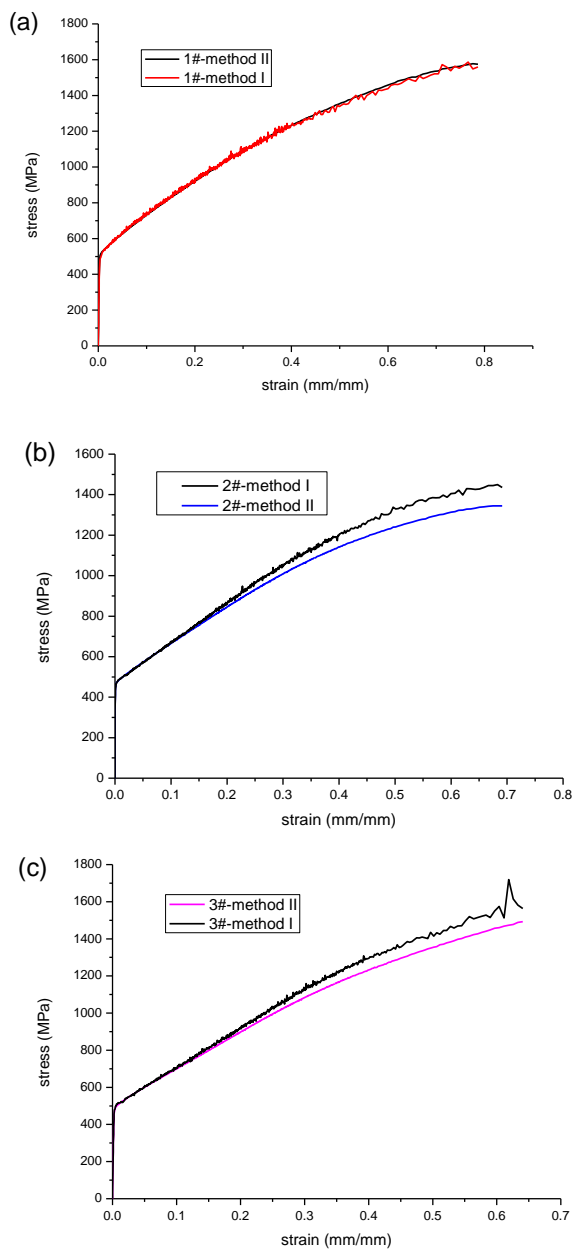


Fig. 6. True stress–strain curves obtained by methods I and II, (a) specimen 1# (b) specimen 2# (c) specimen 3#.

As seen from Fig. 6(b) and (c), the stress at large strain levels calculated by method I is greater than that by method II. The cross-section area obtained by method I is based on the displacements of almost all the points in the cross-section area, while the cross-section area obtained by method II is based on the longitudinal strain of the middle point at the specimen front surface. So the calculation of the true stress by method I includes deformation effects of both the intermediate and marginal positions while the calculation of method II only includes the deformation effect of the middle position. From the profile of the specimen after fracture in Fig. 7, the

deformation at marginal position is a little greater than that at intermediate position. So the area calculated by method I is smaller than that calculated by method II, which is main reason for the stress of method I greater than that of method II.

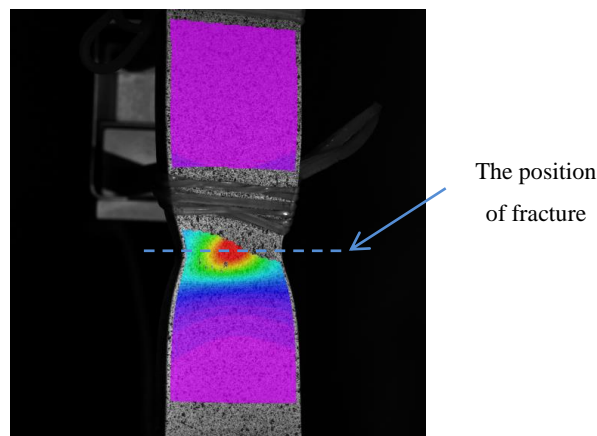


Fig. 7. Strain contours and the fracture position of Specimen 4#

The stress deviations at the ultimate strain are being analyzed on account of the deviations increasing with strain increase. The stress at ultimate strain calculated by method I was compared with that calculated by method II. The comparison results show that deviations at the maximum strain are 0.96%, 6.30% and 4.51% for specimen 1#, 2# and 3#. Although the calculation result of method II is a little conservative, the comparison shows that the deviation is not large between the results of methods I and II. The results of method I are reliable as the calculation procedure is without assumptions, so method II is also a reliable method for the calculation of true stress of pipeline steels. In addition, the calculation results of method II are smooth and stable and it is very convenient to calculate the true stresses of multiple points of one specimen. Method II provides a possibility to test a variety of material properties (such as weld, heat affected zone and base material) on one specimen [14].

3.2 True stress calculation by methods II and III

These three specimens being tested are identified as specimens 4#, 5# and 6#. Six points (five points were align in the center line of the specimen and two points were aligned in a horizontal line at the fracture position) of specimen 4# were researched, which are sketched in Fig. 8. The distance between the points in the center line is 2mm, and 3mm for the points in the horizontal line.

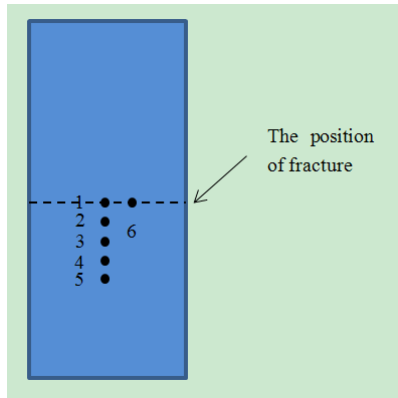


Fig. 8. Positions of the points of specimen 4#. The distance between the points in the center line of the specimen is 2 mm, and 3 mm for the points in the horizontal line

The calculation results of points from 1 to 6 by method II are presented in Fig. 9. The stress-strain curves of points 1 and 6 are coincident, which means that there is small deviation when test the intrinsic material properties through the points in the line of fracture as shown in Fig. 7. Comparison of the results of points from 1 to 5 show that the ultimate strain decreases for points from 1 to 5, and there is a falling section, which is different from the true stress-logarithmic strain curves of points 1 and 6. The strain contours of specimen 4# in the stretching process are shown in Fig. 10, in which stair-step strain contours always exist. The stair-step strain contours are consistent with the ultimate strains of points from 1 to 6. As seen from Fig. 10, the strains of some points, such as point 5, stop increasing from Fig. 10 (d) to (h), that's why there are bifurcations between the curves of point 1 and points from 2 to 5. In theory, that's because there is strain localization at positions of points from 2 to 5 when necking occurs. In another aspect, the results of points from 1 to 6 are in good agreement in small strains, such as 0.1. So method II can get reasonable results from points in the fracture line and get relatively reasonable results from all points under the condition of small strains.

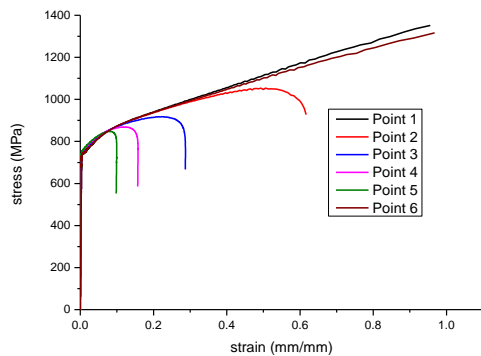


Fig. 9. Stress-strain curves of points from 1 to 6. The ultimate strain decreases for points from 1 to 5 and there is a falling section in the curves of points from 2 to 5

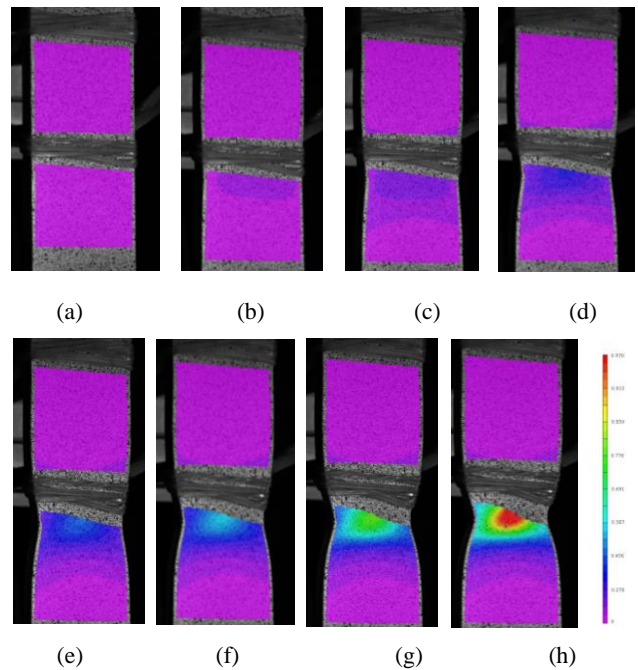


Fig. 10. Contours of strain in different phases of stretching. The stair-step strain contours are consistent with the ultimate strain of points from 1 to 6

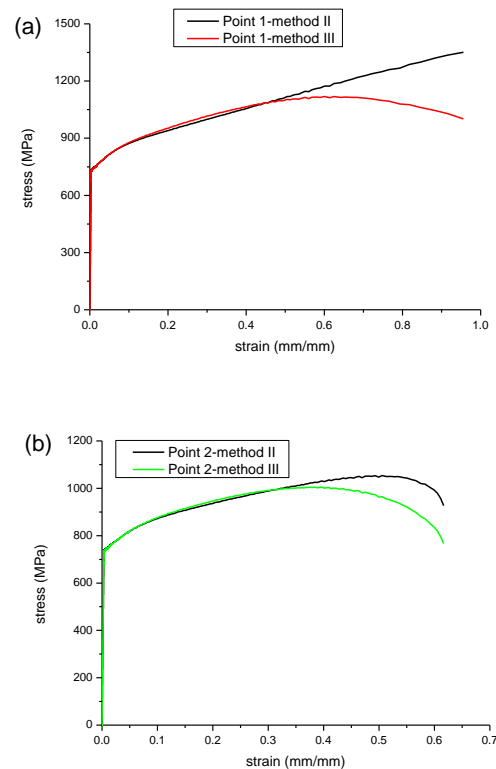


Fig. 11. Calculation results by methods II and III. (a) point 1; (b) point 2

Fig. 11 displays the stress- strain curves of points 1 and 2 by methods II and III. There are bifurcations for

both points. For point 1, there are three phases: these two curves coincide when the strain is less than 0.11; there is a small deviation when the strain is greater than 0.11 but less than 0.46; the deviation is increasing with the strain increase when the strain is greater than 0.46. There are also three phases for points 2. The nominal stress-logarithmic strain curves of points 1 and 2 are presented Fig. 12. The second phases of points 1 and 2 both starts at the onset of necking. The necking happens when the nominal stress drops. This illustrates that method III can obtain the same result as method II before the onset of necking and get an extremely close result after the onset of necking within a certain range of strain, which is 0.46 for point 1 and 0.33 for point 2.

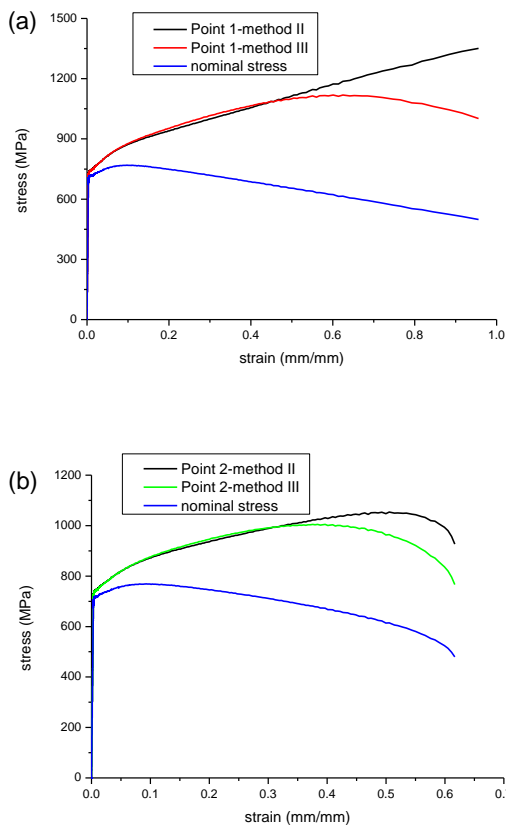


Fig. 12. Nominal stress-true strain curves and true stress-logarithmic strain curves of points 1 and 2. The second phases of points 1 and 2 are all starting at the onset of specimen necking

3.3 Correction of true stress-logarithmic strain curves

The most important part of true stress correction using Bridgman equation and Eq. (7) is to determine the logarithmic strain at the maximum load. The nominal stress-logarithmic strain curves of specimens 1#, 2# and 3# are represented in Fig. 13, in which the logarithmic

strain corresponding to the maximum nominal stress could be obtained. As the maximum load is consistent with the maximum nominal stress, the logarithmic strain at the maximum load can be obtained. And then the plastic part of logarithmic strain at the maximum load can be got by subtracting the elastic part. The plastic logarithmic strains at maximum load of specimens 1#, 2# and 3# are shown in Table 1, which are labeled as $\epsilon_{p_{max}}$. The corrected true stress-logarithmic strain curves of specimens 1#, 2# and 3# are displayed in Fig. 14. The corrected true stresses are little smaller than the directly calculated ones, and the corrected true stress-logarithmic strain curves are flatter than the uncorrected ones in the last section. The average value of the ultimate logarithmic strains and stresses of API-5L X65 are 0.706 and 1366.2MPa, respectively.

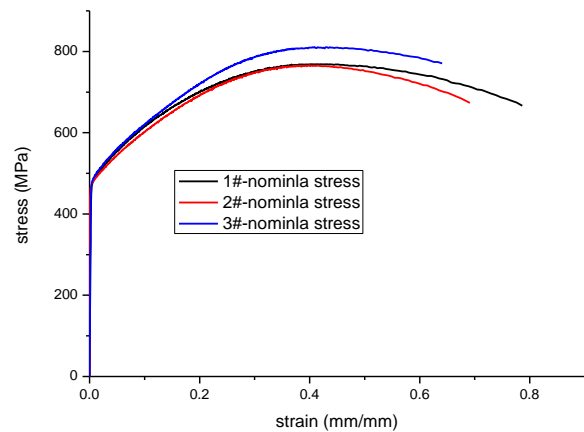


Fig. 13. Nominal stress-logarithmic strain curves of specimens 1#, 2# and 3#. The logarithmic strain at the maximum load can be obtained at the point of the maximum nominal stress

Table 1. Material properties of API-5L X65 and X90

material	Specimen	$\epsilon_{p_{max}}$	ϵ_u	σ_u /MPa
API-5L X65	1#	0.426	0.786	1436.4
	2#	0.403	0.691	1254.0
	3#	0.425	0.641	1408.3
API-5L X90	4#	0.095	0.956	1108.2
	5#	0.068	0.772	1117.2
	6#	0.084	0.976	1027.5

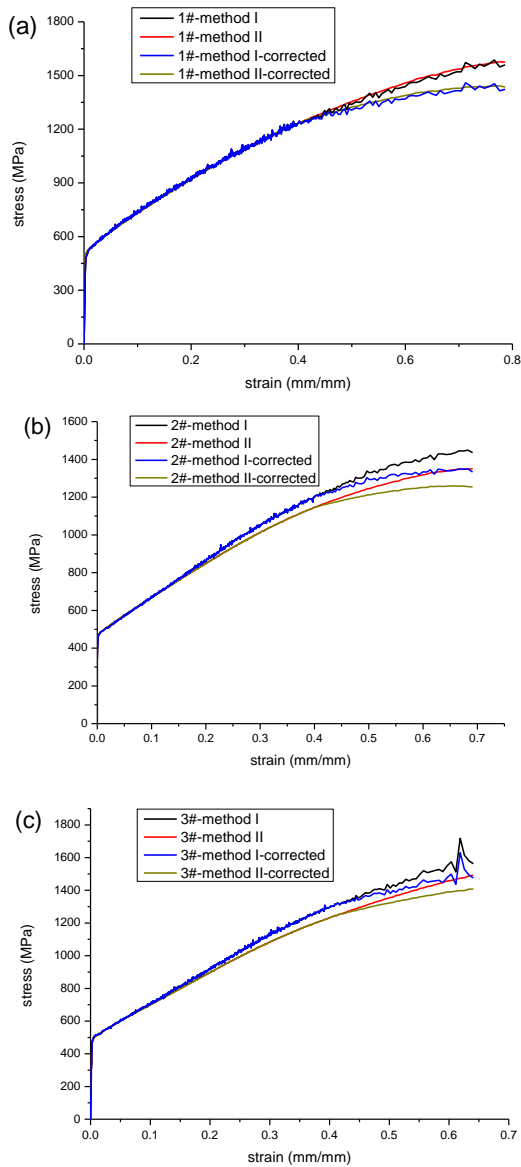


Fig. 14. Corrected true stress-logarithmic strain curves (a) specimen 1#; (b) specimen 2#; (c) specimen 3#. The corrected true stress is little less than the directly calculated true stress

The corrected true stress-logarithmic strain curve of specimen 4#, which material is API-5L X90, is shown in Fig. 15. There are three curves in Fig. 15, which are corrected true stress-logarithmic curve, uncorrected true stress-logarithmic curve and nominal stress-logarithmic strain curve. From the nominal stress-logarithmic strain curve, the plastic logarithmic strain at maximum load can be obtained, which value is 0.095. According to this procedure, the plastic logarithmic strains and uniform elongations of specimens 5# and 6# can be obtained, as shown in Table 1. The average value of uniform elongations of API-5L X90 is 0.082, which is much smaller than that of API-5L X65.

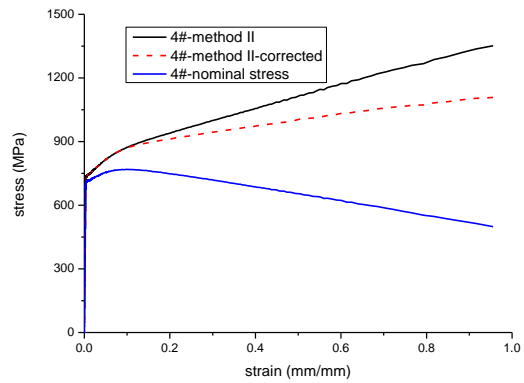


Fig. 15. Corrected true stress-logarithmic curve, uncorrected true stress-logarithmic curve and nominal stress-logarithmic strain curve of specimen 4#

The corrected true stress-logarithmic strain curves of API-5L X90 are shown in Fig. 16. Because the logarithmic strain at the maximum load is small, the deviation between the uncorrected and corrected curves at the ultimate strain is relatively large. The ultimate logarithmic strains and stresses of the three specimens of material API-5L X90 are also included in Table 1. The average value of the ultimate logarithmic strains of API-5L X90 is 0.901 and the average value of the ultimate true stresses is 1084.3MPa.

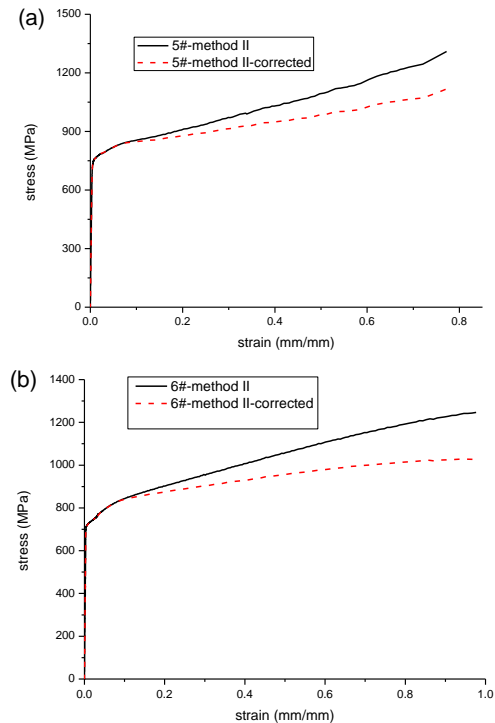


Fig. 16. Corrected true stress-logarithmic strain curves of specimens 5# and 6#. Owing to the smaller logarithmic strain at the onset of necking, the deviation between the uncorrected and corrected curves at the ultimate strain is relatively large

4. Conclusion

Three methods of calculating the true stress are investigated and compared in the process of testing the material properties of pipeline steels with DIC technique. Materials API-5L X65 and X90 are tested. The true stress-logarithmic strain curves are calculated; moreover the correcting process with Bridgman equation is applied. The main conclusions of this study are:

- Method II, which is under the consumption of incompressibility, can also get reasonable results validated by method I. Method II can obtain smooth and stable curves and is convenient to calculate the true stress-logarithmic strain curves of multiple points on one specimen.
- The transverse logarithmic strains were heavily affected by the stress state change from a uniaxial to a complex triaxial stress states.
- The pipeline steel of API-5L X90 has a higher yield stress but a lower ultimate stress than that of API-5L X65. The average uniform elongation of API-5L X65 is greater than that of API-5L X90, but the ultimate logarithmic strain of API-5L X65 is less than that of API-5L X90. The pipeline of API-5L X90 can bear a higher inner pressure with the higher yield stress but has a poor ability to withstand the displacement load.

Acknowledgment

The authors gratefully acknowledge the sponsorship of this work by Specialized Research Fund for the Doctoral Program of Higher Education of China (Grant No. 20100007110006).

References

- [1] ASTM E8M (2004) Standard Test Methods for Tension Testing of Metallic Materials, ASTM, USA.
- [2] Z. L. Zhang, M. Hauge, C. Thaulow, J. Ødegard, Eng. Mech. Fract **69**, 353 (2002).
- [3] E. Berg, E. Østby, C. Thaulow, B. Skallerud, Eng. Mech. Fract **75**, 2352 (2008).
- [4] E. Østby, C. Thaulow, B. Nyhusa, Int J Pressure Vessels Piping **84**, 337 (2007).
- [5] X. Li, Y. Fan, X. Xin, Mater. Mech. Eng **29**, 45 (2005).
- [6] Z. L. Zhang, M. Hauge, J. Odegard, C. Thaulow, Int. J Solids Struct **36**, 3497 (1999).
- [7] M. Jerabek, Z. Major, R. W. Lang, Polym Test **29**, 407(2010).
- [8] E. M. Parsons, M. C. Boyce, D. M. Parks, M. Weinberg, Polym. **46**, 2257(2005).
- [9] E. Parsons, M. C. Boyce, D. M. Parks, Polym. **45**, 2665 (2004).
- [10] J. Kalus, J. K. Jørgensen, Polym. Test **36**, 44 (2014).
- [11] F. Grytten, H. Daiyan, M. Polanco-Loria, S. Dumoulin, Polym. Test **28**, 653 (2009).
- [12] K. J. Han, J. Shuai, X. M. Deng, L. Z. Kong, X. Zhao, M. Sutton, Eng. Mech. Fract **124**, 167 (2014).
- [13] C. Leitão, I. Galvão, R. M. Leal, D. M. Rodrigues, Mater. Des. **33**, 69 (2012).
- [14] W. D. Lockwood, B. Tomaz, A. P. Reynolds, Mater Sci Eng A **323**, 348 (2002).
- [15] W. D. Lockwood, A. P. Reynolds, Mater Sci Eng A **339**, 35–42.
- [16] D. C. William, Fundamentals of Materials Science and Engineering. Fifth Edition (2001).
- [17] ISO 6892-1-2009 (2009) Metallic materials -Tensile testing - Part 1: Method of test at room temperature, ISO, Switzerland.
- [18] GB/T 228-2002 (2002) Metallic Materials - Tensile Testing at Ambient Temperature, State Quality Supervision and Inspection & Quarantine Bureau of P.R.C, China.
- [19] <www.mathworks.com>.
- [20] <www.correlatedsolutions.com>.
- [21] Bridgman PW (1952) Studies in Large Plastic Flow and Fracture. McGraw-Hill, New York.
- [22] G. Le Roy, J. D. Embury, G. Edwards, M. F. Ashby, Acta Metall **29**, 1509 (1981).

*Corresponding author: nature_pma@163.com